# Inter- and intra-event rainfall partitioning dynamics of two typical xerophytic shrubs in the Loess Plateau of China

Jinxia An[1,2], Guangyao Gao[1,2,4], Chuan Yuan[3], Bojie Fu[1,2,4]

[1]State Key Laboratory of Urban and Regional Ecology, Research Center for Eco-Environmental Sciences, Chinese Academy of Sciences, Beijing 100085, China

[2]University of Chinese Academy of Sciences, Beijing 100049, China

[3]State Key Laboratory of Subtropical Silviculture, Zhejiang A&F University, Hangzhou 311300, China

[4]National Observation and Research Station of Earth Critical Zone on the Loess Plateau in Shaanxi, Xi'an 710061, China

*Correspondence to*: Guangyao Gao (gygao@rcees.ac.cn)

**Abstract.** Rainfall is known as the main water replenishment in dryland ecosystem, and rainfall partitioning by vegetation reshapes the spatial and temporal distribution patterns of rainwater entry into the soil. The dynamics of rainfall partitioning have been extensively studied at the inter-event scale, yet very few studies have explored its finer intra-event dynamics and the relating driving factors for shrubs. Here, we conducted a concurrent in-depth investigation of all rainfall partitioning components at inter- and intra-event scales for two typical xerophytic shrubs (*Caragana korshinskii* and *Salix psammophila*) in the Liudaogou catchment of the Loess Plateau, China. The event throughfall (TF), stemflow (SF), and interception loss (IC) and their temporal variations within the rainfall event as well as the

1

25    meteorological factors and vegetation characteristics were systematically measured during

the 2014-2015 rainy seasons. The *C. korshinskii* had significantly higher SF percentage

(9.2%) and lower IC percentage (21.4%) compared to *S. psammophila* (3.8% and 29.5%,

respectively) ($p < 0.05$), but their TF percentages were not significantly different (69.4% vs.

66.7%). At the intra-event scale, TF and SF of *S. psammophila* was initiated (0.1 vs. 0.3 h and

30    0.7 vs. 0.8 h) and peaked (1.8 vs. 2.0 h and 2.1 vs. 2.2 h) more quickly, and TF of *S.

psammophila* lasted longer (5.2 vs. 4.8 h), delivered more intensely (4.3 vs. 3.8 mm·h$^{-1}$),

whereas SF of *C. korshinskii* lasted longer (4.6 vs. 4.1 h), delivered more intensely (753.8 vs.

471.2 mm·h$^{-1}$). For both shrubs, rainfall amount was the most significant factor influencing

inter-event rainfall partitioning, and rainfall intensity and duration controlled the intra-event

35    TF and SF variables. The *C. korshinskii* with larger branch angle, more small branches and

smaller canopy area, has an advantage to produce stemflow more efficiently over *S.

psammophila*. The *S. psammophila* has lower canopy water storage capacity to generate and

peak throughflow and stemflow earlier, and it has larger aboveground biomass and total

canopy water storage of individual plant to produce higher interception loss compared to *C.

40    korshinskii*. These findings contribute to the fine characterization of shrub-dominated

eco-hydrological processes, and improve the accuracy of water balance estimation in dryland

ecosystem.


## 1 Introduction

45    Rainfall is known as the main replenishment of water resources in arid and semi-arid areas,

and water resource is the key factor limiting the function of arid ecosystems (Chesson et al., 2004; Cayuela et al., 2018; Magliano et al., 2019a). Before entering into soil, rainfall is redistributed by plant canopies into throughfall (TF, diffuse water input), stemflow (SF, point water input), and interception loss (IC, evaporation). The sum of TF and SF is defined as "net

50   rainfall". Differences in the distribution of net rainfall caused by plant canopy interception alter the spatial and temporal patterns of rainfall entry into the soil (Martinez-Meza and Whitford, 1996; Li et al., 2009; Van Stan II et al., 2020), and further profoundly affect the water use efficiency of vegetation and ecosystem sustainability (Xu and Li, 2006; Lacombe et al., 2018; Molina et al., 2019). In addition, net rainfall could regulate vegetation

55   physiological metabolic processes through nutrient enrichment (Levia and Frost, 2003; Zhang et al., 2016; Van Stan II et al., 2017; Tonello et al., 2021), ultimately affecting the carbon balance of ecosystems (Chu et al., 2018; Jia et al., 2016). In light of the important role of rainfall partitioning in regulating soil water dynamics and vegetation patch pattern, investigations of the rainfall partitioning dynamics are imperative for a better understanding

60   of the soil-water-vegetation relationships (Molina et al., 2019; Van Stan II et al., 2020; Zhang et al., 2021a).

Studies on rainfall partitioning have been broadly carried out in different climatic zones and various types of vegetation (Gordon et al. 2020; Rivera and Van Stan II, 2020; Zhang et al., 2021b; Yue et al., 2021). Based on a comprehensive global synthesis, Yue et al. (2021)

65   concluded that most TF and SF observations were measured in forests ($n = 718$ and $n = 816$, respectively), and that in shrublands was scarce ($n = 43$ and $n = 63$, respectively), which was

3

mainly due to that the shrubs have multiple branches and the rainfall partitioning of shrubs is difficult to be measured compared to forests. Shrubs are the dominant vegetation type in drylands, providing important ecosystem goods and services (Levia and Frost, 2003; Llorens and Domingo, 2007; Soulsby et al., 2017). However, the lack of information on the detailed dynamics of rainfall partitioning processes induced by shrubs due to limited studies hinders us form a clear understanding of shrubs' eco-hydrological role in shaping and sustaining drylands.

Most of the existing studies on the rainfall partitioning by shrub are based on the inter-event scale (Garcia-Estringana et al., 2010; Magliano et al., 2019a). Magliano et al. (2019a) synthesized that for 27 shrub species in drylands, the mean event-based SF%, TF%, and IC% were 9.4%, 63.0% and 27.6%, respectively. Rainfall partitioning by shrubs has been reported to be determined by various meteorological factors, including rainfall amount, duration and intensity and others (Levia and Frost, 2003; Magliano et al., 2019b) and by vegetation structure characteristics (Martinez-Meza and Whitford, 1996; Garcia-Estringana et al., 2010; Yue et al., 2021). Take the later for example, trees/shrubs with smooth barks, more branches and vertical branching had advantages on SF generation (Honda et al., 2015; Magliano et al., 2019a; Whitworth-Hulse et al., 2020b), and a simple vegetation structure and low canopy density are generally corresponding to a relatively high TF rate and low IC rate (Soulsby et al., 2017; Yue et al., 2021). The complexity of shrub structure poses challenges to understand the causes of rainfall partitioning dynamics under different meteorological conditions, and it is necessary to substantially explore the differences of rainfall partitioning

4

dynamics and main influencing factors among different shrub species (Levia et al., 2010; Sadeghi et al., 2020).

In addition to the inter-event studies, a detailed understanding of shrub rainfall partitioning dynamics at the intra-event scale is essential for better understanding of soil moisture distribution and the hydrological cycle in arid regions. To understand the temporal fluctuations of shrub rainfall partitioning and its importance to hydrological processes, data with high temporal resolution are required (Levia et al., 2010; Levia and Germer, 2015; Cayuela et al., 2018; Zhang et al., 2021a). For instance, Zhang et al. (2018) investigated the spatial-temporal pattern of TF (at 10-min intervals) of *C. korshinskii* in arid area of northern China, highlighting the importance of recording high temporal resolution data. They found that temporal heterogeneity of rainfall clearly affected the spatiotemporal dynamics of TF beneath shrub canopies and wind directions were the main factor affecting TF in different radial directions. Yuan et al. (2019) described the branch SF variability of *C. korshinskii* and *S. psammophil,* and they showed that intra-event branch SF variability of xerophytic shrubs temporally depended on rainfall characteristics, and lag times were longer and more rainfall amount was required to initiate branch SF for *C. korshinskii* than *S. psammophila*. It can be found that those studies on temporal dynamics of shrub rainfall partitioning only explored the single-element process (throughfall or stemflow), and ignored interception loss. Concurrent investigation on all rainfall partitioning components and the associated influencing factors at the intra-event scale have rarely been reported.

This study was designed at the event and process scales to investigate inter-event and

5

删除了：of *C. korshinskii* in arid area of northern China.

删除了：*C. korshinskii* and *S. psammophila*

删除了：.

删除了：the detailed

删除了：process

下移了 [1]: can help better understand and predict the role of shrubs in harvesting rainfall and recharging soil moisture, and thus enhance the understanding of eco-hydrological processes of shrubs (Cayuela et al., 2018; Zhang et al., 2018; Yuan et al., 2019).

intra-event rainfall partitioning variability, based on field measurements on two dominant xerophytic shrubs (*C. korshinskii* and *S. psammophila*) during the rainy seasons of 2014-2015 in the Loess Plateau of China. This study integrated the inter-event and intra-event dynamics of rainfall partitioning by combining TF, SF and IC at the individual plant scale. We mainly seek to (a) compare the dynamic processes of rainfall partitioning between the two shrubs at both inter-event and intra-event scales, and (b) elucidate the effects of rainfall characteristics and vegetation structure characteristics on rainfall partitioning at both scales. This work can help better understand and predict the role of shrubs in harvesting rainfall and recharging soil moisture, and thus enhance the understanding of eco-hydrological processes of shrubs.

## 2 Materials and methods

### 2.1 Site description and experimental design

This study was carried out in the Liudaogou catchment (110°21′-110°23′ E, 38°46′-38°5′ N) in Shenmu county, Shaanxi Province of China (Fig. 1a). The Liudaogou catchment (6.9 km$^2$, altitude from 1094 to 1273 m) is located between the northern Loess Plateau and the south fringe of Mu Us sandy land in North China. This region is characterized by a moderate temperate continental climate with well-defined rainy and dry seasons. The mean annual rainfall is 437 mm ranging between 109-891 mm (dataset between 1971-2013), and the potential evaporation is 1337 mm yr$^{-1}$ (Jia et al., 2013). Approximately 70-80% of the rainfall events are concentrated in the warm months between July and September and most of them occur in the form of torrential rain (Yang et al., 2019). The Liudaogou catchment was characterized by the natural arid scrub steppe before it was artificially vegetated in the past

20 or 30 years for soil and water conservation, windbreak and sand fixation. The main land use types include artificial grassland, artificial shrub and farmland, and the main vegetation species are *Stipa bungeana*, *C. korshinskii* and *S. psammophila*, which are widely distributed in the arid and semiarid areas of northwestern China (Yuan et al., 2019).

Two representative xerophytic shrubs, *C. korshinskii* and *S. psammophil*a with 20 years old, were used for the study. Both species are multiple-stemmed deciduous perennial shrubs with inverted cone crowns and without trunks. They have minimal nutrient requirements, extensive adaptability and strong stress resistance, which makes them superior in adapting to resource-poor environments. According to the documentation of *Flora of China* (Chao and Gong, 1999; Liu et al., 2010) and field observations, the *S. psammophila* has an odd number of strip-shaped leaves with 2-4 mm in width and 40-80 mm in length, and the *C. korshinskii* has pinnate compound leaves arranged opposite or sub-opposite with 6-10 cm in length, and each pinna has 5 to 8 pairs of ovate leaflets (7-8 mm in length and 2-5 mm in width). We established two plots (one for *C. korshinskii* and the other for *S. psammophila*) at the southwestern catchment for field observation (Fig. 1a). The two plots share similar stand conditions, with the sizes of 3294 m$^2$ and 4056 m$^2$, elevations of 1179 m and 1207 m, and slopes of 13º and 18º, respectively. The distance between the two plots do not exceed 1.5 km.

**2.2 Field measurements**

**2.2.1 Measurements of rainfall and meteorological factors**

This study focused on the individual shrub rainfall partitioning of *C. korshinskii* and *S. psammophila* during the 2014-2015 rainy seasons. Gross rainfall was measured using one

删除了：(Chao and Gong, 1999; Liu et al., 2010)

7

tipping bucket rain gauge (TBRG, with 186.3 cm$^2$ collection area) (Onset® RG3-M, Onset

Computer Corp., USA) in the open areas, which was recorded every 0.2 mm by a datalogger

(Fig. 1b). The rainfall characteristics, e.g., rainfall amount (RA, mm), rainfall duration (RD,

h), rainfall interval (RI, h), average rainfall intensity (I, mm·h$^{-1}$), rainfall intensity at 10-min

interval (I$_{10}$, mm·h$^{-1}$) were calculated accordingly. For I$_{10}$, the one after the onset of rainfall is

defined as I$_{10\_b}$ (mm·h$^{-1}$), and the maximum I$_{10}$ during the rainfall process is defined as I$_{10\_max}$

(mm·h$^{-1}$). As the TBRG has a resolution of 0.2 mm, we define a single rainfall event as one

that is greater than 0.2 mm and not raining for at least 4 hours apart (Iida et al., 2012). A

meteorological station was set up at the experimental plot to record wind speed (WS, m·s$^{-1}$)

and wind direction (WD, º) (Model 03002, R. M. Young Company, Traverse City, Michigan,

USA), air temperature (T, ºC) and relative humidity (H, %) (Model HMP 155, Vaisala,

Helsinki, Finland), which were logged at 10-min interval by a data logger (Model CR1000,

Campbell Scientific, Inc., USA).

### 2.2.2 Measurements of vegetation characteristics

Three representative shrub plants with similar crown heights and crown areas were selected

in each shrub species (Table 1). Based on plot investigation, the vegetation traits at the scale

of single plant and branch were measured. For each plant, we measured shrub height (SH, m)

with a graduated telescopic stick, counted the number of branches (NB), and calculated the

projected canopy area (CA, m$^2$) by measuring canopy diameter following the south-north and

east-west direction. The total number of branches was 143 and 218 for selected *C. korshinskii*

and *S. psammophila* plants, respectively. For each branch, we measured branch length (BL,

cm) with a measuring tape, branch angle (BA, º) with a pocket geologic compass, and branch diameter (BD, mm) with a vernier caliper to calculate the total basal area of the shrub (TBA, $m^2$). Thus, four BD categories (0-10, 10-15, 15-20 and > 20 mm) were defined to ensure the appropriate branch amounts within each category. The measured vegetation traits of *C. korshinskii* and *S. psammophila* plants are shown in Table 1.

Water storage capacity of the canopy is a key factor in determining the amount of interception loss (Levia and Herwitz, 2005; Garcia-Estringana et al., 2010) and SF yield (Van Stan II et al., 2020). We selected 10 representative branches for each shrub species outside the stands, to determine the canopy water storage capacity (C, mL/g) using water immersion method (Garcia-Estringana et al., 2010; Wang et al., 2012). The C was calculated as the difference between saturated weight and fresh weight divided by the dry biomass of the selected branch. The *C. korshinskii* and *S. psammophila* had a C of 0.85 mL/g and 0.38 mL/g, respectively. In addition, we estimated the total dry aboveground biomass of single plant (TB) for each species according to the allometric growth model developed by Yuan et al. (2017) in the same study area. The total canopy water storage of single plant ($C_m$ = TB times C) was calculated to represent the amount of rainfall absorbed by the shrub canopy during the rainfall event (Table 1).

### 2.2.3 Measurements of inter-event rainfall partitioning

Manual rain gauges (314.12 $cm^2$ collection area) were used to measure event TF at eight radial directions (E, SE, S, SW, W, NW, N, NE) beneath each shrub canopy (Fig. 1b). For *C. korshinskii*, eight TF gauges were placed under each *C. korshinskii* plant with 50 cm distance

from the base of stems in the eight directions. For *S. psammophila*, twenty TF gauges were placed under each plant, with twelve of them placed in 50 cm, 100 cm, and 150 cm distances from the base of stems in four directions (E, S, W, and N), and eight of them placed in 75 cm

220 and 125 cm distances in the other four directions (SE, SW, NW, and NE). If the rainfall ended during the daytime, we completed the collection of TF samples within two hours after the end of rainfall. If the rainfall ended at night, we completed the collection of samples as early as possible in the next day to avoid evaporation.

A total of 53 branches of *C. korshinskii* (17, 21, 7, 8 for BD categories of 0-10, 10-15,

225 15-20 and > 20 mm, respectively) and 98 branches of *S. psammophila* (20, 30, 20 and 28 for BD categories of 0-10, 10-15, 15-20, and > 20 mm, respectively) were used to determine SF yield. Funnels constructing of flexible aluminum foil plates were used to collect SF (Fig. 1b). The funnel was fixed to each branch near the base and sealed with neutral silicone caulk, and a 0.5 cm diameter PVC hose was attached vertically to transport SF from the funnel to a

230 container with a lid (SF gauges) with minimum travel time.

**2.2.4 Measurements of intra-event rainfall partitioning**

Among the selected plants, one *C. korshinskii* and one *S. psammophila* plant were selected to record the volume and timing of TF and SF with TBRGs at intra-event scale. A TBRG was installed in each of four radial directions (E, S, W, N) beneath the shrub canopy of each

235 species, to measure the temporal variations of TF within the rainfall event (Fig. 1b). And for each species, we selected six representative branches to characterize intra-event SF dynamics through strict selection conditions, including no crossover between the experimental branch

删除了: four

删除了: of the four BD categories (0-10, 10-15, 15-20, and > 20 mm, respectively)…

10

and adjacent branches, no inflection point from the tip to the base of the branch, and easy of measurement. These branches were distributed across the four BD categories (0-10, 10-15, 15-20, and > 20 mm, respectively). Due to missing or incomplete measured data, four branches were finally identified for each species, located in each of the four BD categories to

245 measure intra-event SF (6.7, 13.5, 18.6, and 22.1 mm for *C. korshinskii* and 7.2, 14.4, 18.2, and 31.3 mm for *S. psammophila*). SF TBRGs were covered with the polyethylene films to prevent the accessing of throughfall and splash (Fig. 1b).

### 2.3 Rainfall partitioning calculations

### 2.3.1 Inter-event rainfall partitioning calculations

250 For each individual shrub, we measured TF volume for each TF gauges, averaged them, and then converted the volume into TF depth ($TF_d$, mm) at each rainfall event. And the percentage of TF (TF%, %) was calculated by dividing $TF_d$ by the RA, and the average TF intensity (TFI, mm·h$^{-1}$) was calculated by dividing $TF_d$ by the TF duration (TFD, h). The TFD was recorded by TF TBRGs.

255     The inter-event SF yield was defined as the total SF volume of a single plant in a rainfall event. The SF volumes measured on the selected branches were averaged to obtain the average volume of SF on the branch scale, which multiply the number of branches to obtain the total SF volume from the plant. The shrub-scale SF equivalent water depth ($SF_d$, mm) and the average SF intensity (SFI, mm·h$^{-1}$) were calculated. The percentage of SF (SF%, %) was

260 converted by dividing $SF_d$ by the RA. The $SF_d$ and SFI were calculated by the following equations (Hanchi and Rapp, 1997; Levia and Germer, 2015):

删除了：at each rainfall event

11

$$SF_d = \left(\overline{SF_b} \times n\right)\big/\left(1000 \times CA\right) \tag{1}$$

$$SFI = \left(\overline{SF_b} \times n\right)\big/\left(10 \times TBA \times SFD\right) \tag{2}$$

where $\overline{SF_b}$ (ml) is the average volume of SF on the branch scale, $n$ is the number of branches of individual plant, CA ($m^2$) is the canopy area of individual plant, TBA ($cm^2$) is the total basal area of individual plant, and SFD is SF duration (h) recorded by SF TBRGs. The parameters 1000 and 10 are the unit conversion factor.

The IC depth ($IC_d$, mm) and percentage of IC (IC%, %) were estimated as:

$$IC_d = RA\text{-}TF_d\text{-}SF_d \tag{3}$$

$$IC\% = 100\%\text{-}TF\%\text{-}SF\% \tag{4}$$

The above inter-event rainfall partitioning variables and their explanations are summarized in Table 2.

### 2.3.2 Intra-event rainfall partitioning calculations

The TF and SF volume and timing within rainfall event were automatically recorded at dynamic intervals between neighboring TBRG tips (0.2 mm). To better reflect fluctuations in rainfall partitioning components, the intra-event TF and SF data were aggregated every 10 minutes. The four TF depths recorded by TBRGs were averaged to obtain the average TF depth at 10-min interval ($TF_{d10}$, mm). The TF intensity at 10-min interval ($TFI_{10}$, mm·$h^{-1}$) was calculated by dividing the $TF_{d10}$ by the 10 min. Meanwhile, SF depth ($SF_{d10}$, mm) and SF intensity at 10-min interval ($SFI_{10}$, mm·$h^{-1}$) were calculated as:

$$SF_{d10} = \sum_{j=1}^{4}\left(186.3 \times SF_{RG,j} \times n_j\right)\big/\left(100 \times CA\right) \tag{5}$$

删除了: The calculations of intra-event rainfall partitioning are based on the data recorded by TBRG every 10 minutes, including temporal dynamics of TF and SF for individual plant. …

删除了: TF depth at 10-min interval ($TF_{d10}$, mm)

删除了: , which was recorded by TF TBRGs

12

$$SFI_{10} = \sum_{j=1}^{4} \left( 186.3 \times SF_{RG,j} \times n_j \right) \Big/ (TBA \times 1/6) \qquad (6)$$

290　where $SF_{RG,j}$ (mm) is the SF depth of the selected $j$th category branch recorded by TBRG at

10-min interval (1/6 h), $n_j$ is the number of branches in the $j$th category of single plant, 4 is

the number of BD category (0-10, 10-15, 15-20, and > 20 mm), and 186.3 ($cm^2$) is the

collection area of TBRG. The product of $SF_{RG,j}$ and 186.3 is the SF volume from the branch.

The parameter 100 is the unit conversion factor.

295　　　Based on the calculated $TFI_{10}$ and $SFI_{10}$, the maximum TF and SF intensity at 10-min

interval ($TFI_{10\_max}$ and $SFI_{10\_max}$, respectively, mm·h$^{-1}$) of each rainfall event can be

determined. The descriptive variables for the intra-event rainfall partitioning also include the

lag times of TF or SF corresponding to the rainfall event. Based on the temporal data

recorded by TBRGs (between neighboring tips), the following variables were calculated:

300　$LG_{TF}$ and $LG_{SF}$ (h), the time lag of TF and SF generation after the start of rainfall,

respectively; $LM_{TF}$, $LM_{SF}$ and $LM_R$ (h), the time lag of $TFI_{10\_max}$, $SFI_{10\_max}$ and $I_{10\_max}$ relative

to the onset of rainfall, respectively; and $LE_{TF}$ and $LE_{SF}$ (h), the time lag of TF and SF ending

after the end of rainfall. The intra-event rainfall partitioning variables and their explanations

are summarized in Table 2.

305　**2.4 Statistical analysis**

Independent-samples T-tests were used to analyze differences in rainfall partitioning

parameters between *C. korshinskii* and *S. psammophila* at both inter-event and intra-event

scales. To detect the effects of meteorological factors on rainfall partitioning, Pearson

correlation analysis was used to test the significance between rainfall partitioning parameters

13

and meteorological factors at the two scales. The significant correlated factors were double-checked by partial correlation analysis to determine their individual effects on rainfall partitioning components. Stepwise regression of these indicators was performed by analytical tests at the 0.05 level of significance to select the most influential factors on rainfall partitioning variables at inter-event and intra-event scales, and the corresponding quantitative relationships were established based on a qualifying level of significance ($p < 0.05$) and the highest coefficient of determination ($R^2$). Significance levels were set at 95% confidence intervals. Data analysis was performed using SPSS 21.0, Origin 2018, and Excel 2019.

## 3  Results

### 3.1 Inter-event variations of rainfall partitioning

#### 3.1.1 Characteristics of inter-event rainfall partitioning variables

A total of 38 rainfall events were recorded for rainfall partitioning measurements, including 20 events (215.4 mm) in 2014 and 18 events (205.6 mm) in 2015, which accounted for 75.2% and 75.0% of total rainfall amount during the experimental period in 2014 and 2015, respectively (Fig. 2a). The RA ranged from 1.2-41.9 mm with an average of 11.1 ± 8.8 mm (mean ± standard). In general, rainfall events were unevenly distributed in terms of RA. Approximately 34.2% of rainfall events were smaller than 5 mm, 26.3% within 5-10 mm, 26.3% within 10-20 mm, and 13.2% larger than 20 mm, representing 8.8%, 17.5%, 36.3%, and 37.4% of the total rainfall amount, respectively (Fig. 2a). The average I varied from 0.2 mm·h$^{-1}$ to 35.1 mm·h$^{-1}$ with an average of 6.0 ± 1.3 mm·h$^{-1}$, and approximately 76.3% of the events was < 5 mm·h$^{-1}$, 13.2% was 5–10 mm·h$^{-1}$, and 10.5% was > 10 mm·h$^{-1}$. $I_{10\_max}$

14

ranged from 1.2 mm·h$^{-1}$ to 68.4 mm·h$^{-1}$ with an average of 13.7 ± 2.7 mm·h$^{-1}$, and approximately 42.1% of the events was < 5 mm·h$^{-1}$, 23.7% was 5–10 mm·h$^{-1}$, and 34.2% was > 10 mm·h$^{-1}$. The RD ranged from 0.2 h to 28.9 h and averaged 5.3 ± 1.0 h. The RD of most rainfall events was less than 5 h (68.4%), and only 5 rainfall events had RD greater than 10 h.

The TF$_d$ for *C. korshinskii* ranged from 0.7 mm to 31.2 mm (coefficient of variation, CV = 87.5%) with corresponding TF% ranging from 54.0 to 80.3% (CV = 10.6) across the 38 events (Fig. 2b). The TF$_d$ values for *S. psammophila* were 0.4-33.4 mm (CV = 96%) and 28.5-82.7% (CV = 21.5%), respectively (Fig. 2c). The SF$_d$ for *C. korshinskii* ranged from 0.04 mm to 6.1 mm (CV = 106.6%), with corresponding SF % of 2.0-14.5% (CV = 34.2%) (Fig. 2b). The comparable SF$_d$ values for *S. psammophila* varied from 0.01 mm to 2.2 mm (CV = 98.6%) and 0.7-5.9% (CV = 38.9%), respectively (Fig. 2c). The IC$_d$ values for *C. korshinskii* varied from 0.5 mm to 2.9 mm (CV = 43.9%), with corresponding IC% of 5.7-40.8% (CV = 47.3%) (Fig. 2b), and the comparable values were 0.8-5.7 mm (CV = 44.8%) and 12.1-70.8% (CV = 53.3%) for *S. psammophila*, respectively (Fig. 2c). For *C. korshinskii*, TF represented the largest component of all rainfall events, while for *S. psammophila*, SF represented the smallest component of all rainfall events (Figs. 2 b and 2c).

The percentages of TF, SF, and IC in rainfall partitioning between two species are shown in Fig. 3. There was no significant difference ($p$ > 0.05) in average TF% between *C. korshinskii* (69.4 ± 7.4%) and *S. psammophila* (66.7 ± 14.6%). The SF% was significantly higher ($p$ < 0.05) for *C. korshinskii* (9.2 ± 3.2%) than *S. psammophila* (3.8 ± 1.5%) (Fig. 3b).

The IC% was significantly lower ($p < 0.05$) for *C. korshinskii* (21.4 ± 10.2%) than *S. psammophila* (29.5 ± 15.9%) (Fig. 3c). The variations of TF% and IC% among the rainfall events were greater for *S. psammophila*, but that of SF% was smaller compared to *C. korshinskii* (Fig. 3).

### 3.1.2 Relationships between inter-event rainfall partitioning variables and meteorological factors

Correlation analysis indicated that meteorological factors had a similar effect on rainfall partitioning for the two species. Stepwise regression analysis identified that the SF parameters ($SF_d$ and SF%), TF parameters ($TF_d$ and TF%) and IC parameters ($IC_d$ and IC%) were all mainly controlled by RA. Following RA, the influences of rainfall intensity (I, $I_{10\_max}$) were also significant ($p < 0.05$). However, the other meteorological factors (RD, RI, WS, WD, T, H) had no significant effect on rainfall partitioning ($p > 0.05$).

Significantly positive and linear relationships were found between $TF_d$ and RA for both *C. korshinskii* and *S. psammophila* (Fig. 4a). According to the regression equations, the threshold of rainfall amount for TF generation was 0.8 and 1.1 mm for *C. korshinskii* and *S. psammophila*, respectively. The TF% increased with increasing RA as an exponential function (Fig. 4b). When the RA reached 20 mm, the increasing of TF% became stabilized, and TF% of *C. korshinskii* and *S. psammophila* reached 79.2% and 80.0%, respectively. The $SF_d$ also had a significantly positive and linear relationship with RA for the two species (Fig. 4c). When RA was greater than 1.7 mm and 2.2 mm, *C. korshinskii* and *S. psammophila* began to produce SF, respectively. The SF% increased exponentially with increasing RA, and

SF% of *C. korshinskii* was always higher than that of *S. psammophila*. The SF% approximately tended to be constant at 12.2% and 5.5% as RA $\geq$ 20 mm for *C. korshinskii* and *S. psammophila*, respectively (Fig. 4d). The $IC_d$ was also positively correlated with RA (Fig. 4e). However, IC% decreased exponentially with incremental RA, and IC% of *S. psammophila* was always higher than that of *C. korshinskii* (Fig. 4f). When RA reached 20 mm, IC% approximately tended to be constant at 9.0% and 14.5% for *C. korshinskii* and *S. psammophila*, respectively.

### 3.2 Intra-event variations of rainfall partitioning

删除了: 3

### 3.2.1 Characteristics of intra-event rainfall partitioning variables

删除了: 3

The intra-event TF and SF were well synchronized with rainfall process, in terms of the shape, number and location of the intensity peaks for both *C. korshinskii* and *S. psammophila*, which was vividly demonstrated at representative four rainfall events in Fig. 5. The SF intensity ($SFI_{10}$) was much higher than TF intensity ($TFI_{10}$) and rainfall intensity ($I_{10}$) for both *C. korshinskii* and *S. psammophila*, whereas $TFI_{10}$ was less than or equal to $I_{10}$. As expected, IC was the main component at the initial stage of rainfall, and then TF was the major component ($\geq$ 50%) for rainfall partitioning (Fig. 5). As the continue of rainfall, the cumulative amount of TF, SF and IC increases, and finally the percentage of cumulative amounts (TF, SF, and IC) over the cumulative rainfall stabilized near a fixed value. The TF and SF generation thresholds measured using the TBRGs were 0.4 ± 0.2 mm and 1.0 ± 0.7 mm for *C. korshinskii*, and 0.3 ± 0.1 mm and 0.7 ± 0.3 for *S. psammophila*, respectively. They were expected to be both smaller than the thresholds derived from the regression equation between $TF_d$ (or $SF_d$) and

删除了: The cumulative rainfall partitioning in Fig. 5 showed thatAs expected,

17

400 <span style="color:red">RA aforementioned which assume that TF and SF start after the canopy is fully wet. This further demonstrates the importance of high-resolution data in rainfall partitioning studies.</span>

Fig. 6 describes the difference in average intra-event TF and SF variables between *C korshinskii* and *S. psammophila*. Although there were no statistically significant differences between the two species in intensities, durations, or the lag time of TF and SF, some trends

405 were observed. The TFI and $TFI_{10\_max}$ of both species were similar to I ($6.0 \pm 1.3$ mm/h) and $I_{10\_max}$ ($13.7 \pm 2.7$ mm/h), respectively. In contrast, SFI and $SFI_{10\_max}$ were significantly greater than I and $I_{10\_max}$, respectively. Specifically, TFI and $TFI_{10\_max}$ of *C. korshinskii* were $3.8 \pm 1.2$ mm·h$^{-1}$ and $13.3 \pm 4.9$ mm·h$^{-1}$, respectively, which were slighter lower than that of *S. psammophila* ($4.3 \pm 1.5$ mm·h$^{-1}$ and $14.6 \pm 5.5$ mm·h$^{-1}$, respectively) (Fig. 6a). The SFI

410 and $SFI_{10\_max}$ of *C. korshinskii* ($753.8 \pm 208.0$ mm·h$^{-1}$ and $3627.2 \pm 1424.7$ mm·h$^{-1}$, respectively) were higher than those of *S. psammophila* ($471.2 \pm 170.2$ mm·h$^{-1}$ and $1424.8 \pm 538.3$ mm·h$^{-1}$, respectively) (Fig. 6b).

Furthermore, a time lag was usually observed between the onset of rainfall and the generation of TF ($LG_{TF}$) and SF ($LG_{SF}$). Similarly, there is a time lag between rainfall and TF

415 or SF in terms of the time to reach maximum intensity (LM) and the time to end (LE). The *S. psammophila* had a shorter lag time than *C. korshinskii* in terms of TF ($LG_{TF}$: $0.1 \pm 0.04$ h vs. $0.3 \pm 0.1$ h) and SF production ($LG_{SF}$: $0.7 \pm 0.3$ h vs. $0.8 \pm 0.3$ h), and their reaching maximum intensity ($LM_{TF}$: $1.8 \pm 0.8$ h vs. $2.0 \pm 0.6$ h; $LM_{SF}$: $2.1 \pm 0.7$ h vs. $2.2 \pm 0.5$ h) (Figs. 6c and 6d). However, the *S. psammophila* had longer TF duration ($5.2 \pm 1.4$ h vs. $4.8 \pm 1.4$ h)

420 and $LE_{TF}$ ($0.2 \pm 0.1$ h vs. $0.1 \pm 0.1$ h) than *C. korshinskii* (Fig. 6c). Conversely, the SF

18

duration and LE$_{SF}$ in *C. korshinskii* (4.6 ± 1.4 h and 0.4 ± 0.1 h, respectively) were longer than those in *S. psammophila* (4.1 ± 1.3 h and 0.2 ± 0.2 h, respectively) (Fig. 6d). The above differences in TF and SF variables indicate that *S. psammophila* should be more conducive to generate TF than *C. korshinskii*, while *C. korshinskii* should be more conducive to produce SF than *S. psammophila*.

### 3.2.2 Relationships between intra-event rainfall partitioning variables and meteorological factors

Similar relationships existed between intra-event rainfall partitioning variables and meteorological factors for two species. For both shrubs, rainfall intensity (I, I$_{10\_max}$, and I$_{10\_b}$) and RD were the main influencing factors affecting intra-event TF variables (Fig. 7) and SF variables (Fig. 8). While the effects of other meteorological factors (RD, RI, WS, WD, T, H) on TF and SF variables within the event were not significant ($p > 0.05$). The TFI, TFI$_{10\_max}$, LM$_{TF}$, and TFD were linearly correlated with I, I$_{10\_max}$, LM$_R$, and RD, respectively, while LG$_{TF}$ was power functionally correlated with I$_{10\_b}$ ($p < 0.05$). The TF intensities (TFI and TFI$_{10\_max}$) of *S. psammophila* increased faster with rainfall intensities (I and I$_{10\_max}$) than that of *C. korshinskii*. The SFI, SFI$_{10\_max}$, LM$_{SF}$, and SFD were also linearly correlated with I, I$_{10\_max}$, LM$_R$, and RD, respectively ($p < 0.05$). The LG$_{SF}$ was power functionally correlated with I$_{10\_b}$ ($p = 0.14$ and $p = 0.16$ for *C. korshinskii* and *S. psammophila*, respectively), which was weaker than the correlation between LG$_{TF}$ with I$_{10\_b}$. The SF intensities (SFI and SFI$_{10\_max}$) of *C. korshinskii* increased with rainfall intensities (I and I$_{10\_max}$) more rapidly than that of *S. psammophila*. However, for both species, there was no significant relationship

删除了: 3.3

删除了: significantly

19

between LE$_{TF}$ or LE$_{SF}$ and RD (Figs. 7 and 8). The above results indicate that the intra-event

rainfall partitioning variables largely dependent on rainfall intensity and duration.

## 4    Discussion

### 4.1 Rainfall partitioning and influencing factors at inter-event scale

This study indicated that SF% of *C. korshinskii* (9.2%) was significantly higher than that of *S. psammophila* (3.8%) (Fig. 3), which was comparable to the value of 10.4% and 6.3% reported by Yang et al. (2019) for the same species in similar semiarid regions of China. Under the same rainfall regimes, the difference in vegetation characteristics is the main reason for the difference in SF (Yuan et al., 2017; Whitworth-Hulse et al., 2020a; Yue et al., 2021). Comparing the structural properties of two shrubs with the same age (20 years), we found that CA, BD, BL, BA and NB values of *S. psammophila* were 4.51, 1.61, 1.94, 0.83 and 1.52 times of those of *C. korshinskii*, respectively (Table 1). On the branch scale, *C. korshinskii* had more small and short branches, but larger BA than that of *S. psammophila*, which was contributed to SF generation. Yuan et al. (2016) concluded that a beneficial branch architecture for SF production should include more relatively small branches and larger branch angles, and SF productivity decreased with BD size of branches. Furthermore, *C. korshinskii* with a smaller CA, and it had a larger SF$_d$ than *S. psammophila* under the same SF volume. Somewhat in line with Yuan et al. (2016) and Yue et al. (2021), our results suggest that a beneficial branch architecture for SF production of *C. korshinskii* should include relatively small CA, BD, BL and large BA (Table 1).

Leaf traits had been reported to exert a significant influence on rainfall partitioning

**删除了:** This study indicated that SF% and IC% significantly differed between the two xerophytic shrub species in the Loess Plateau, northern China (Fig. 3). …

**删除了:** rainfall partitioning

(Garcia-Estringana et al., 2010; Magliano et al., 2019a). According to the documentation in *Flora of China* (Liu et al., 2010), *C. korshinskii* has pinnate compound leaves and each pinna has 5 to 8 pairs of ovate leaflets, and the leaves are lanceolate and concave, and the surface is densely sericeous. In comparison, *S. psammophila* has stripe or stripe oblanceolate leaves, margin revolute, and which upper surface of mature leaf blade is almost glabrous (Chao and Gong, 1999). The branches of both shrubs are smooth, with a more developed cuticle layer on the surface of the *S. psammophila* branches, while the *C. korshinskii* branches contain oil and have waxy skin (Chao and Gong, 1999; Liu et al., 2010). The leaf morphology and epidermal characteristics of branches of *C. korshinskii* was more beneficial for SF generation than that of *S. psammophila* (Whitworth-Hulse et al., 2020b; Yuan et al. 2017). It was found that big biomass of leaves, concave leaf shape and leaf pubescence are beneficial to promote the generation of SF (Yuan et al., 2016). These factors together enable the leaves to function as a highly efficient natural water collecting system.

The mean IC% of *C. korshinskii* (21.4%) was significantly lower than that of *S. psammophila* (29.5%) in this study. The intercepts in the fitted formulas between interception loss and rainfall amount in Fig. 4e indicated that *C. korshinskii* (0.92 mm) had a lower canopy water storage than *S. psammophila* (1.15 mm), hence the potential interception loss of *C. korshinskii* was lower. Zhang et al. (2017) reported that IC% were higher in the *H. rhamnoides* stand (24.9%) than in the *S. pubescens* stand (19.2%), which was mainly attributed to the lower canopy water storage of *S. pubescen*. This study was done at the shrub-scale, so we compared the total canopy water storage of individual plant ($C_m$), and we

found that $C_m$ of *S. psammophila* (6.0 L) was significantly higher than that of *C. korshinskii*

(3.9 L) (Table 1). This was mainly due to the significantly higher average total dry

aboveground biomass of *S. psammophila* (15.7 kg per plant) than *C. korshinskii* (4.6 kg per

plant). Consequently, individual *S. psammophila* absorbed more rain water to moisten the

branches and leaves than that of individual *C. korshinskii*, which could explain higher IC% of

*S. psammophila* than *C. korshinskii*. Thus, the best predictors for interception loss were

biomass-related parameters (i.e., woody biomass and total biomass) (Li et al., 2016).

## 4.2 Rainfall partitioning and influencing factors at intra-event scale

Temporal heterogeneity of rainfall clearly influences the amount and timing of TF and SF

reaching the soil under the canopy, as explained by some previous intra-event rainfall

partitioning studies from forested ecosystems (Owens et al., 2006; Levia et al., 2010; Molina

et al., 2019). Our experiment investigated the intra-event dynamics of all rainfall partitioning

components in xerophytic shrubs, which has rarely been reported before. Our results showed

that the temporal dynamics of TF and SF under the shrub canopy almost matched the

dynamics of rainfall (Fig. 5). It agreed with the reports of Zhang et al. (2018) and Yuan et al.

(2019) who demonstrated the temporal synchronization of TF and SF with rainfall,

respectively. The SF intensity is generally greater than rainfall intensity for different species

(Fig. 6), which has eco-hydrological significance (Spencer and van Meerveld, 2016). The SF

converges substantial rainwater to the shrub bases and then delivers it into the soil as a point

input to recharge soil moisture (Germer et al., 2010; Cayuela et al., 2018; Jian et al., 2019).

We assume that changes in SF inputs explain, at least in part, the temporal variation in

515　subsurface moisture patterns. Spatial and temporal patterns in rainfall partitioning may influence various eco-hydrological processes under canopies, such as local soil moisture dynamics in arid and semi-arid regions (Li et al., 2009; Wang et al., 2011; Jian et al., 2019; Molina et al., 2019; Zhang et al., 2018).

　　The intensity variables and lag time of SF and TF relative to rainfall were the key to
520　describe the intra-event rainfall partitioning (Fig. 6). The effects of meteorological factors on SF and TF variables at the intra-event scale were derived from multiple regression analysis in this study. The SF and TF variables (intensity and temporal dynamics) were strongly influenced by rainfall intensity (e.g., I, $I_{10\_max}$ and $I_{10\_b}$) and duration (e.g., RD and $LM_R$). This is consistent with the results reported by Yuan et al. (2019) who indicated that there was
525　a significant effect of rainfall intensity on the stemflow process of *C. korshinskii*. The main factors affecting intra-event SF and TF variables were the same, but the effects were still slightly different between the two shrubs. Under the same rainfall intensity, the average TF intensity under the canopy of *S. psammophila* was higher than *C. korshinskii* (Figs. 7a and 7b). But the average SF intensity of *C. korshinskii* was greater than *S. psammophila* at shrub
530　scale (Figs. 8a and 8b), which was also found for the branch SF intensity reported by Yuan et al. (2019). In addition to the inter-shrub differences, the effects of $I_{10\_b}$ on $LG_{TF}$ and $LG_{SF}$ were slightly different. The correlation between $LG_{SF}$ and $I_{10\_b}$ (Fig. 8c) was weaker than that between $LG_{TF}$ and $I_{10\_b}$ (Fig. 7c). This may be due to the fact that TF has two components, i.e., free TF and released TF (Staelens et al., 2008; Levia et al., 2017; Van Stan II et al., 2020),
535　and that SF only starts to produce when a certain amount of rainfall is reached (Germer et al.,

删除了: , while

2010; Levia et al., 2010; Dunkerley, 2014; Yuan et al., 2019). Our results indicated that *S. psammophila* had dynamic characteristics (e.g., larger TFI, TFI$_{10}$ and LE$_{TF}$ as well as TFD, and shorter LG$_{TF}$ and LM$_{TF}$) producing larger TF depth (TFd = TFI*TFD) (Figs. 6a and 6c),

540    while *C. korshinskii* had dynamic characteristics (e.g., larger SFI, SFI$_{10}$ and LE$_{SF}$ as well as SFD) producing larger SF depth (SFd = SFI*SFD) (Figs. 6b and 6d).

The vegetation characteristics have an important effect on the dynamics and the lag time of TF and SF (Yuan et al., 2019; Zhang et al., 2018). Based on the temporal data recorded by TBRGs, we found that *C. korshinskii* produced TF and SF later than *S. psammophila* (Figs. 5

545    and 6), which was reported by Yuan et al. (2019) for branch SF of the same species. We inferred that this was due to the higher canopy water storage capacity of *C. korshinskii* (0.85 mL/g) compared to *S. psammophila* (0.38 mL/g). However, when the branches were moistened, SF production of *C. korshinskii* was greater than that of *S. psammophila* because of its branch and leaf characteristics as discussed in subsection 4.1 (Fig. 5). It was found that

550    the great bark water storage capacity of forests could result in the further delay of TF and SF onset (Levia and Herwitz, 2005; Levia et al., 2010; Li et al., 2016; Pinos et al., 2021). The different intra-event TF and SF variables between species were attributed to a complex interaction of biotic and abiotic factors (Yuan et al., 2019; Zhang et al., 2018; Levia et al., 2010).

555    **4.3 Implications and further scopes**

Most of previous rainfall partitioning investigations for shrubs were limited at inter-event scale, or only focused on TF or SF at intra-event scale. The intra-event rainfall partitioning dynamics,

24

删除了: that were beneficial to the generation of

删除了: which were beneficial to the generation of

删除了: Data from

删除了: 10-min rainfall partitioning records indicated

删除了: and we

删除了: ). We also found that during the accumulative rainfall partitioning, accumulative TF% of *S. psammophila* occasionally exceeded 100% (Fig. 6d), which was due to the drip effect of the canopy (Zhang et al., 2018; Whitworth-Hulse et al., 2020a)....

which could help have a better understanding of soil water replenishment and its distribution in soil and the key ecohydrological cycle in in drylands, have been rarely explored. This study is the first time to investigate all the rainfall partitioning components (i.e., TF, SF and IC) for shrubs at both inter- and intra-event scales, which steps further and provides a full view of the reciprocal dynamics among interception loss, throughfall, and stemflow at the shrub-scale. This is the main novelty and a step forward compared with the previous related studies. We have also obtained the quantitative relationship between rainfall partitioning variables and rainfall characteristics, and further elaborated the influence of vegetation structure characteristics (leaf, canopy structure, and biomass, etc..) on rainfall partitioning. The obtained new insights help to understand the fine characterization of shrub-dominated eco- hydrological processes, and improve the accuracy of water balance estimation in dryland ecosystem.

This study investigated the inter- and intra-event rainfall partitioning dynamics of two typical xerophytic shrubs in the Loess Plateau of China. There are several issues that need further investigation. Firstly, long-term observations of rainfall partitioning dynamics for more shrub plants and species are needed, and the rainfall partitioning models should be developed for shrubs. Secondly, the effects of rainfall partitioning on soil moisture dynamics, nutrient cycling, and plant transpiration should be substantially investigated to detect the interactions between water redistribution and vegetation physiological processes. Finally, the extension from the individual plant to stand and more larger scale remains a challenging topic for rainfall partitioning, which can help improve understanding the role of rainfall partitioning in the regional hydrologic cycle.

## 5 Conclusions

590 In this study, we analyze the rainfall partitioning and the influences of bio-/abiotic factors of two typical shrubs at both inter- and intra-event scales in the Loess Plateau. To ensure a larger proportion of the rainfall is allocated under the canopy, two species can obtain more net rainfall through different mechanisms. At the event scale, there was no significant difference in TF percentage between the two shrubs, but *C. korshinskii* had significantly higher SF percentage

595 and lower IC percentage compared to *S. psammophila*. At the intra-event scale, TF and SF of two shrubs were well synchronized with the rainfall, but *C. korshinskii* had the advantage of stemflow production, while *S. psammophila* had the advantage of TF generation. For both shrubs, the inter-event rainfall partitioning amount and percentage depended more on rainfall amount, and rainfall intensity and duration controlled the intra-event TF and SF variables.

600 The *C. korshinskii* has larger branch angles, more small branches and smaller canopy areas to produce SF more efficiently, and *S. psammophila* has larger biomass to intercept more rainfall amount. These findings could enhance our understanding of TF and SF dynamics and corresponding driving factors at inter- and intra-event scales, and help in modelling the critical eco-hydrological processes in arid and semi-arid regions.

605

**Data availability:** The data that support the findings of this study are available from the corresponding author upon request.

**Author contributions:** JXA: Formal analysis, Investigation, Methodology, Writing - original

26

610 draft; GYG: Conceptualization, Methodology, Writing - review & editing; CY: Investigation, Writing - review & editing; BJF: Writing - review & editing.

**References**

Cayuela, C., Llorens, P., Sanchez-Costa, E., Levia, D. F., and Latron, J.: Effect of biotic and abiotic factors on inter- and intra-event variability in stemflow rates in oak and pine stands 625 in a Mediterranean mountain area, J. Hydrol., 560, 396-406, 2018.

Chao, P. N. and Gong, G. T.: *Salix* (*Salicaceae*), in: Flora of China, edited by: Wu, Z. Y., Raven, P. H., and Hong, D. Y., Science Press, Beijing and Missouri Botanical Garden Press, St. Louis, 162–274, 1999.

Chesson, P., Gebauer, R. L., Schwinning, S., Huntly, N., Wiegand, K., Ernest, M. S., Sher, A., 630 Novoplansky, A., and Weltzin, J. F.: Resource pulses, species interactions, and diversity

maintenance in arid and semi-arid environments, Oecologia, 141, 236-253, 2004.

Chu, X., Han, G., Xing, Q., Xia, J., Sun, B., Yu, J. B., and Li, D.: Dual effect of precipitation redistribution on net ecosystem $CO_2$ exchange of a coastal wetland in the Yellow River Delta, Agr. Forest Meteorol., 249, 286-296, 2018.

635 Dunkerley, D.: Stemflow production and intrastorm rainfall intensity variation: an experimental analysis using laboratory rainfall simulation, Earth. Surf. Proc. Land., 39, 1741-1752, 2014.

Garcia-Estringana, P., Alonso-Blázquez, N., and Alegre, J.: Water storage capacity, stemflow and water funneling in Mediterranean shrubs, J. Hydrol., 389, 363-372, 2010.

640 Germer, S., Werther, L., and Elsenbeer, H.: Have we underestimated stemflow? Lessons from an open tropical rainforest, J. Hydrol., 395, 169-179, 2010.

Gordon, D. A., Coenders-Gerrits, M., Sellers, B. A., Sadeghi, S. M. M. and Van Stan II, J. T.: Rainfall interception and redistribution by a common North American understory and pasture forb, Eupatorium capillifolium (Lam. dogfennel), Hydrol. Earth. Syst. Sci., 24, 645 4587–4599, 2020.

Hanchi, A., and Rapp, M.: Stemflow determination in forest stands, Forest Ecol. Manage., 97, 231-235, 1997.

Honda, E. A., Mendonça, A. H., and Durigan, G.: Factors affecting the stemflow of trees in the Brazilian Cerrado, Ecohydrology, 8, 1351-1362, 2015.

650 Iida, S., Shimizu, T., Kabeya, N., Nobuhiro, T., Tamai, K., Shimizu, A., Ito, E., Ohnuki, Y., Abe, T., Tsuboyama, Y., Chann, S., and Keth, N.: Calibration of tipping-bucket flow meters and

rain gauges to measure gross rainfall, throughfall, and stemflow applied to data from a Japanese temperate coniferous forest and a Cambodian tropical deciduous forest, Hydrol. Process., 26, 2445-2454, 2012.

655 Jia, X. X., Shao, M. A., Wei, X. R., and Wang, Y. Q.: Hillslope scale temporal stability of soil water storage in diverse soil layers, J. Hydrol., 498, 254-264, 2013.

Jia, X., Zha, T. S., Gong, J. N., Wang, B., Zhang, Y. Q., Wu, B., Qin, S. G., and Peltola, H.: Carbon and water exchange over a temperate semi-arid shrubland during three years of contrasting precipitation and soil moisture patterns, Agr. Forest Meteorol., 228, 120-129,

660 2016.

Jian, S. Q., Hu, C. H., Zhang, G. D., and Zhang, J. P.: Study on the throughfall, stemflow, and interception of two shrubs in the semiarid Loess region of China, Agr. Forest Meteorol., 279, 107713, 2019.

Lacombe, G., Valentin, C., Sounyafong, P., de Rouw, A., Soulileuth, B., Silvera, N., Pierret, A.,

665 Sengtaheuanghoung, O., and Ribolzi, O.: Linking crop structure, throughfall, soil surface conditions, runoff and soil detachment: 10 land uses analyzed in Northern Laos, Sci. Total Environ., 616-617, 1330-1338, 2018.

Levia, D. F. and Frost, E. E.: A review and evaluation of stemflow literature in the hydrologic and biogeochemical cycles of forested and agricultural ecosystems, J. Hydrol., 274, 1-29,

670 2003.

Levia, D. F. and Germer, S.: A review of stemflow generation dynamics and stemflow-environment interactions in forests and shrublands, Rev. Geophys., 53, 673-714,

删除了: .,

删除了: .,

删除了: .,

删除了: .,

2015.

Levia, D.F. and Herwitz, S. R.: Interspecific variation of bark water storage capacity of three deciduous tree species in relation to stemflow yield and solute flux to forest soils, Catena, 64, 117-137, 2005.

Levia, D.F.,Hudson, S. A., Llorens, P., and Nanko, K.: Throughfall drop size distributions: a review and prospectus for future research, WIREs Water, 4, 2017.

Levia, D. F., Van Stan II, J. T., Mage, S. M., and Kelley-Hauske, P. W.: Temporal variability of stemflow volume in a beech-yellow poplar forest in relation to tree species and size, J. Hydrol., 380, 112-120, 2010.

Li, X., Xiao, Q. F., Niu, J. Z., Dymond, S., van Doorn, N. S., Yu, X. X., Xie, B. Y., Lv, X. Z., Zhang, K. B., and Li, J.: Process-based rainfall interception by small trees in Northern China: The effect of rainfall traits and crown structure characteristics, Agr. Forest Meteorol., 218-219, 65-73, 2016.

Li, X. Y., Yang, Z. P., Li, Y. T., and Lin, H.: Connecting ecohydrology and hydropedology in desert shrubs: stemflow as a source of preferential flow in soils, Hydrol. Earth. Syst. Sci., 13, 1133-1144, 2009.

Liu, Y. X., Chang, Z. Y. and Gennady, P. Y.: *Caragana* (*Fabaceae*), in: Flora of China, edited by: Wu, Z. Y., Raven, P. H., and Hong, D. Y., Science Press, Beijing and Missouri Botanical Garden Press, St. Louis, 528–545, 2010.

Llorens, P. and Domingo, F.: Rainfall partitioning by vegetation under Mediterranean conditions. A review of studies in Europe, J. Hydrol., 335, 37-54, 2007.

700  Magliano, P. N., Whitworth-Hulse, J. I., and Baldi, G.: Interception, throughfall and stemflow partition in drylands: Global synthesis and meta-analysis, J. Hydrol., 568, 638-645, 2019a.

Magliano, P. N., Whitworth-Hulse, J. I., Florio, E. L., Aguirre, E. C., and Blanco, L. J.: Interception loss, throughfall and stemflow by Larrea divaricata: The role of rainfall

705      characteristics and plant morphological attributes, Ecol. Res., 34, 753-764, 2019b.

Martinez-Meza, E., Whitford, W. G.: Stemflow, throughfall and channelization of stemflow by roots in three Chihuahuan desert shrubs, J. Arid Environ., 32, 271-287, 1996.

Molina, A. J., Llorens, P., Garcia-Estringana, P., Moreno de Las Heras, M., Cayuela, C., Gallart, F., and Latron, J.: Contributions of throughfall, forest and soil characteristics to

710      near-surface soil water-content variability at the plot scale in a mountainous Mediterranean area, Sci. Total Environ., 647, 1421-1432, 2019.

Owens, M. K., Lyons, R. K., and Alejandro, C. L.: Rainfall partitioning within semiarid juniper communities: effects of event size and canopy cover, Hydrol. Process., 20, 3179-3189, 2006.

715  Pinos, J., Latron, J., Levia, D. F., and Llorens, P.: Drivers of the circumferential variation of stemflow inputs on the boles of Pinus sylvestris L. (Scots pine), Ecohydrology, 14, 2021.

Rivera, D. N, and Van Stan II, J. T.: Grand theft hydro? Stemflow interception and redirection by neighbouring Tradescantia ohiensis Raf. (spiderwort) plants, Ecohydrology, 13, 2020.

Sadeghi, S. M. M., Gordon, D. A., and Van Stan II, J. T.: A Global Synthesis of Throughfall and

720      Stemflow Hydrometeorology. In: Van Stan II, J. T., Gutmann, E., Friesen, J. (Eds.),

Precipitation Partitioning by Vegetation, Springer Nature Switzerland, Cham, pp. 49-70, 2020.

Soulsby, C., Braun, H., Sprenger, M., Weiler, M., and Tetzlaff, D.: Influence of forest and shrub canopies on precipitation partitioning and isotopic signatures, Hydrol. Process., 31, 4282-4296, 2017.

Spencer, S. A. and van Meerveld, H. J.: Double funnelling in a mature coastal British Columbia Forest: spatial patterns of stemflow after infiltration, Hydrol. Process., 30, 4185-4201, 2016.

Staelens, J., De Schrijver, A., Verheyen, K., and Verhoest, N.E.C.: Rainfall partitioning into throughfall, stemflow, and interception within a single beech (Fagus sylvatica L.) canopy: influence of foliation, rain event characteristics, and meteorology, Hydrol. Process., 22, 33-45, 2008.

Tonello, K. C., Rosa, A. G., Pereira, L. C., Matus, G. N., Guandique, M. E. G., and Navarrete, A. A.: Rainfall partitioning in the Cerrado and its influence on net rainfall nutrient fluxes, Agr. Forest Meteorol., 303, 108372, 2021.

Van Stan II, J. T., Gutmann, E., and Friesen, J. (Eds.): Precipitation Partitioning by Vegetation — A Global Synthesis, Precipitation Partitioning by Vegetation, Springer Nature Switzerland, 2020.

Van Stan II, J. T., Wagner, S., Guillemette, F., Whitetree, A., Lewis, J., Silva, L., and Stubbins, A.: Temporal Dynamics in the Concentration, Flux, and Optical Properties of Tree-Derived Dissolved Organic Matter in an Epiphyte-Laden Oak-Cedar Forest, Journal

725

730

735

740

删除了: .,

删除了: .D

删除了: .:

of Geophysical Research, 122, 2982-2997, 2017.

Wang, X. P., Zhang, Y. F., Hu, R., Pan, Y. X., and Berndtsson, R.: Canopy storage capacity of xerophytic shrubs in Northwestern China, J. Hydrol., 454, 152-159, 2012.

Wang, X., Wang, Z., Berndtsson, R., Zhang, Y., and Pan, Y.: Desert shrub stemflow and its significance in soil moisture replenishment, Hydrol. Earth. Syst. Sci., 15, 561-567, 2011.

Whitworth-Hulse, J. I., Magliano, P. N., Zeballos, S. R., Gurvich, D. E., Spalazzi, F., and Kowaljow, E.: Advantages of rainfall partitioning by the global invader Ligustrum lucidum over the dominant native Lithraea molleoides in a dry forest, Agr. Forest Meteorol., 290, 108013, 2020a.

Whitworth-Hulse, J. I., Magliano, P. N., Zeballos, S. R., Aguiar, S., and Baldi, G.: Global patterns of rainfall partitioning by invasive woody plants, Global Ecol. Biogeogr., 30, 235-246, 2020b.

Xu, H. and Li, Y.: Water-use strategy of three central Asian desert shrubs and their responses to rain pulse events, Plant and Soil, 285, 5-17, 2006.

Yang, X. L., Shao, M. A., and Wei, X. R.: Stemflow production differ significantly among tree and shrub species on the Chinese Loess Plateau, J. Hydrol., 568, 427-436, 2019.

Yuan, C., Gao, G. Y., and Fu, B. J.: Stemflow of a xerophytic shrub (Salix psammophila) in northern China: Implication for beneficial branch architecture to produce stemflow, J. Hydrol., 539, 577-588, 2016.

Yuan, C., Gao, G. Y., and Fu, B. J.: Comparisons of stemflow and its bio-/abiotic influential factors between two xerophytic shrub species, Hydrol. Earth. Syst. Sci., 21, 1421-1438,

删除了: Aguiar, S., Baldi, G.

2017.

Yuan, C., Gao, G. Y., Fu, B. J., He, D. M., Duan, X. W., and Wei, X. H.: Temporally dependent
effects of rainfall characteristics on inter- and intra-event branch-scale stemflow
variability in two xerophytic shrubs, Hydrol. Earth. Syst. Sci., 23, 4077-4095, 2019.

Yue, K., De Frenne, P., Fornara, D. A., Van Meerbeek, K., Li, W., Peng, X., Ni, X., Peng, Y.,
Wu, F., Yang, Y., and Penuelas, J.: Global patterns and drivers of rainfall partitioning by
trees and shrubs, Glob Chang Biol, 27, 3350-3357, 2021.

Zhang, H., Fu, C., Liao, A., Zhang, C., Liu, J., Wang, N., and He, B.: Exploring the stemflow
dynamics and driving factors at both inter- and intra-event scales in a typical subtropical
deciduous forest, Hydrol. Process., 35, 2021a.

Zhang, Y., Li, X. Y., Li, W., Wu, X. C., Shi, F. Z., Fang, W. W., and Pei, T. T.: Modeling rainfall
interception loss by two xerophytic shrubs in the Loess Plateau, Hydrol. Process., 31,
1926-1937, 2017.

Zhang, Y. F., Wang, X. P., Hu, R., and Pan, Y. X.: Meteorological influences on process-based
spatial-temporal pattern of throughfall of a xerophytic shrub in arid lands of northern
China, Sci. Total Environ., 619-620, 1003-1013, 2018.

Zhang, Y. F., Wang, X. P., Pan, Y. X., and Hu, R.: Variations of Nutrients in Gross Rainfall,
Stemflow, and Throughfall Within Revegetated Desert Ecosystems, Water Air and Soil
Pollution, 227, ARTN 183, 2016.

Zhang, Y. F., Wang, X. P., Pan, Y. X., Hu, R., Chen, N., and Sandel, R. O.: Global quantitative
synthesis of effects of biotic and abiotic factors on stemflow production in woody

ecosystems, Global Ecol. Biogeogr., 30, 1713-1723, 2021b.

790

**Table 1.** Descriptive statistics (mean ± standard error) of canopy morphology of *C. korshinskii* (CK1-CK3) and *S. psammophila* (SP1-SP3) plants. Values are mean ± SD.

| Plant ID | SH (m) | CA (m²) | NB | BL (cm) | BA (°) | BD (mm) | TBA (cm²) | TB (kg) | $C_m$ (L) |
|----------|--------|---------|-----|---------|--------|---------|-----------|---------|-----------|
| CK1 | 2.2 | 5.3 | 47 | 150.6±5.1 | 60.26±2.6 | 9.2±0.5 | 34.9 | 4.0 | 3.4 |
| CK2 | 2.3 | 5.2 | 47 | 123.3±6.6 | 65.5±2.1 | 8.5±0.5 | 31.3 | 3.6 | 3.1 |
| CK3 | 2.4 | 5.3 | 49 | 134.6±6.7 | 65.4±4.4 | 9.9±0.7 | 45.8 | 6.2 | 5.2 |
| Average | 2.3a | 5.27a | 48a | 136.2a | 63.77a | 9.2a | 37.3a | 4.6a | 3.9a |
| SP1 | 3.5 | 23.9 | 85 | 262.2±6.0 | 67.1±1.4 | 13.8±0.5 | 139.7 | 14.3 | 5.4 |
| SP2 | 3.3 | 26.1 | 55 | 268.0±7.7 | 56.0±3.1 | 15.1±0.6 | 124.3 | 15.9 | 6.0 |
| SP3 | 3.6 | 21.4 | 78 | 262.0±7.8 | 35.1±2.9 | 15.3±0.5 | 155.9 | 17.0 | 6.5 |
| Average | 3.5b | 23.8b | 73b | 264.1b | 52.7a | 14.8b | 140.0b | 15.7b | 6.0b |

Note: SH: shrub height; CA: canopy area; NB: number of branches; BL: branch length; BA: branch angle; BD: basal diameter of branch; TBA: total basal area of the shrub; TB: total dry aboveground biomass; $C_m$: total canopy storage per plant. Different letters indicate statistically significant differences between two species ($p < 0.05$).

**Table 2.** Rainfall partitioning parameters at inter- and intra-event scales.

| Scale | Parameter (unit) | Explanation |
|---|---|---|
| Inter-event | $TF_d$ (mm) | Throughfall depth per rainfall event |
| | $SF_d$ (mm) | Stemflow depth per rainfall event |
| | $IC_d$ (mm) | Interception loss depth per rainfall event |
| | TF% | Percentage of TF per rainfall event |
| | SF% | Percentage of SF per rainfall event |
| | IC% | Percentage of IC per rainfall event |
| | TFD (h) | Throughfall duration |
| | SFD (h) | Stemflow duration |
| | TFI (mm·h$^{-1}$) | Average throughfall intensity |
| | SFI (mm·h$^{-1}$) | Average stemflow intensity |
| Intra-event | $I_{10}$ (mm·h$^{-1}$) | Rainfall intensity at 10-min interval |
| | $I_{10\_max}$ (mm·h$^{-1}$) | Maximum $I_{10}$ during the rainfall process |
| | $TFI_{10}$ (mm·h$^{-1}$) | Throughfall intensity at 10-min interval |
| | $TFI_{10\_max}$ (mm·h$^{-1}$) | Maximum $TFI_{10}$ during the rainfall process |
| | $SFI_{10}$ (mm·h$^{-1}$) | Stemflow intensity at 10-min interval |
| | $SFI_{10\_max}$ (mm·h$^{-1}$) | Maximum $SFI_{10}$ during the rainfall process |
| | $LG_{TF}$ (h) | Time lag of throughfall generation after the start of rainfall |
| | $LG_{SF}$ (h) | Time lag of stemflow generation after the start of rainfall |
| | $LM_R$ (h) | Time lag of $I_{10\_max}$ occurrence relative to the onset of rainfall |
| | $LM_{TF}$ (h) | Time lag of $TFI_{10\_max}$ occurrence relative to the onset of rainfall |
| | $LM_{SF}$ (h) | Time lag of $SFI_{10\_max}$ occurrence relative to the onset of rainfall |
| | $LE_{SF}$ (h) | Time lag of throughfall ending after the end of rainfall |
| | $LE_{SF}$ (h) | Time lag of stemflow ending after the end of rainfall |
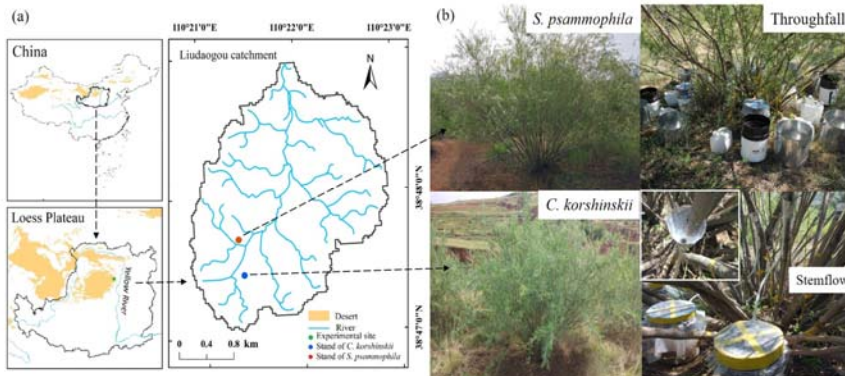
800　**Figure 1.** The location and experimental settings in the plots of *C. korshinskii* and *S. psammophila.*
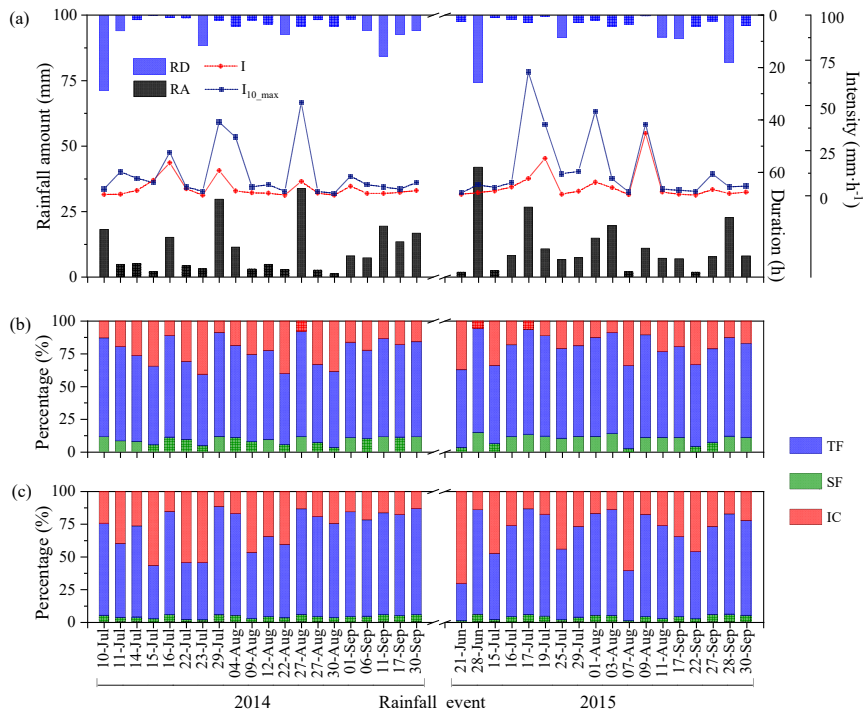
**Figure 2**. (a) individual rainfall amount (RA) ($n$ = 38), rainfall duration (RD), average rainfall intensity (I, mm·h$^{-1}$), maximum rainfall intensity in 10 minutes (I$_{10\_max}$, mm·h$^{-1}$); and rainfall partitioning into TF %, SF %, and IC % of (b) *C. korshinskii* and (c) *S. psammophila*.
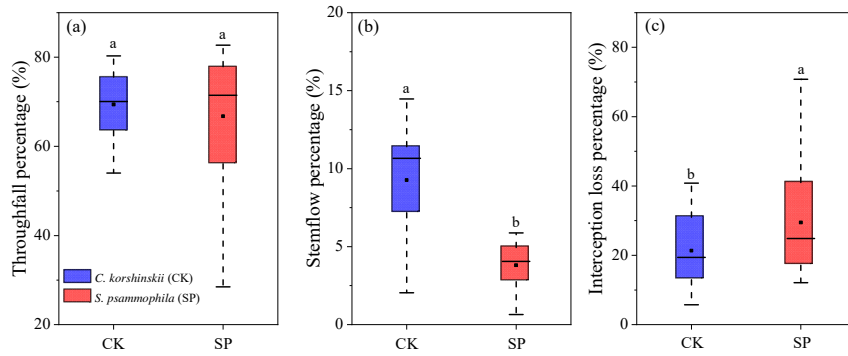
**Figure 3**. Box-plots of (a) TF%, (b) SF%, and (c) IC% for *C. korshinskii* (CK) and *S.*
*psammophila* (SP). The horizontal thick black line indicates the median, boxes correspond to
the 25th and 75th percentiles, and whiskers represent values that fall within 1.5 times the
interquartile range. Mean values are represented with the black square. Different letters
indicate significant differences between the two species ($p < 0.05$).
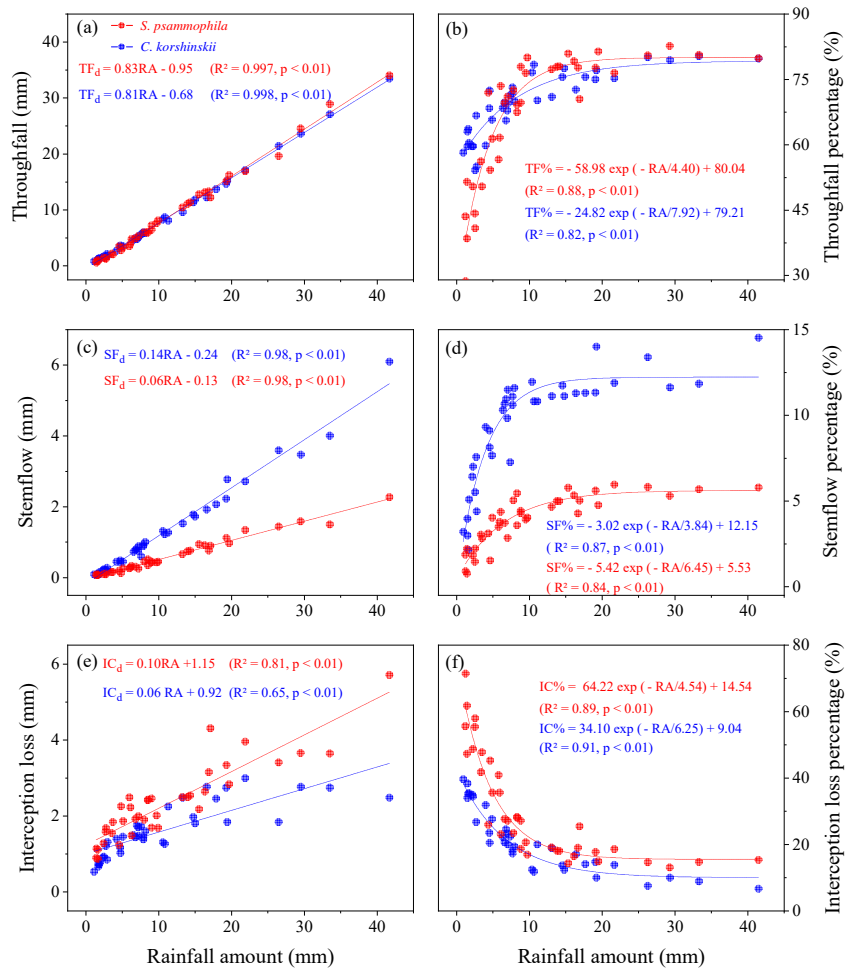
815

**Figure 4.** Inter-event rainfall partitioning as a function of individual rainfall amount for *C. korshinskii* and *S. psammophila*.
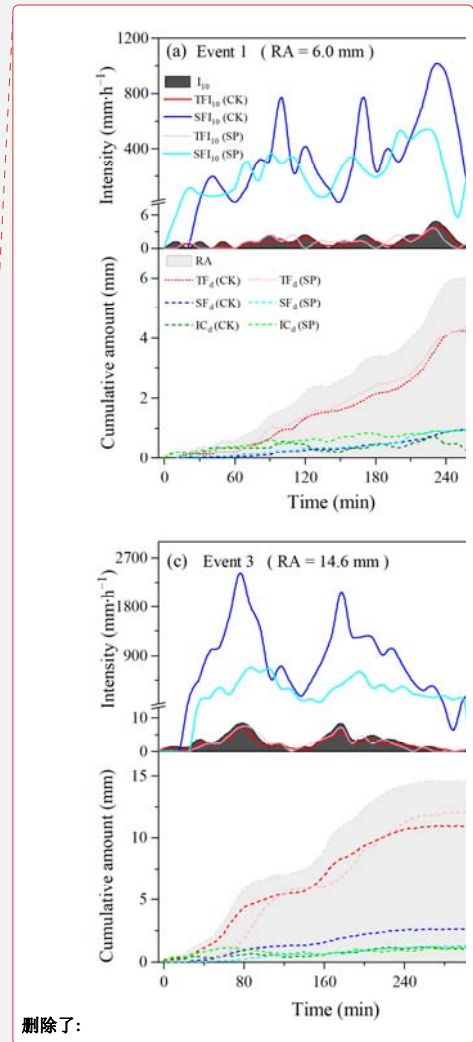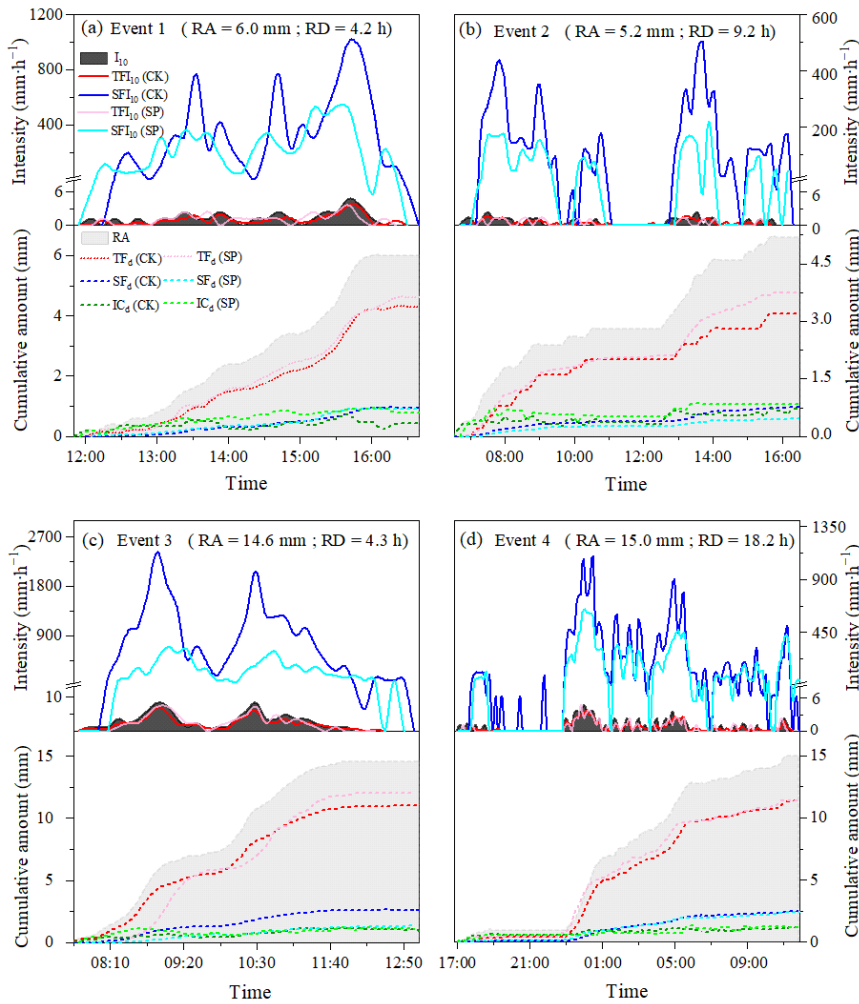
**Figure 5.** Time series (10-min interval) of rainfall partitioning within four rainfall events for *C. korshinskii* (CK) and *S. psammophila* (SP). Events 1-4 occurred on August 3, September 17, September 28, and September 30 in 2015, respectively. The solid lines represent the rainfall, TF and SF intensity at 10-min interval. The dotted lines indicate the accumulated amount of RA, TF, SF, and IC.
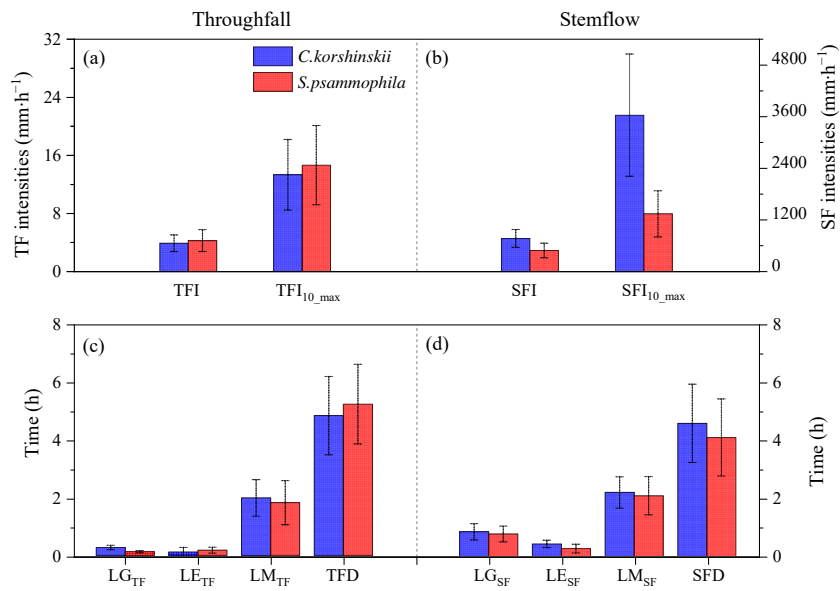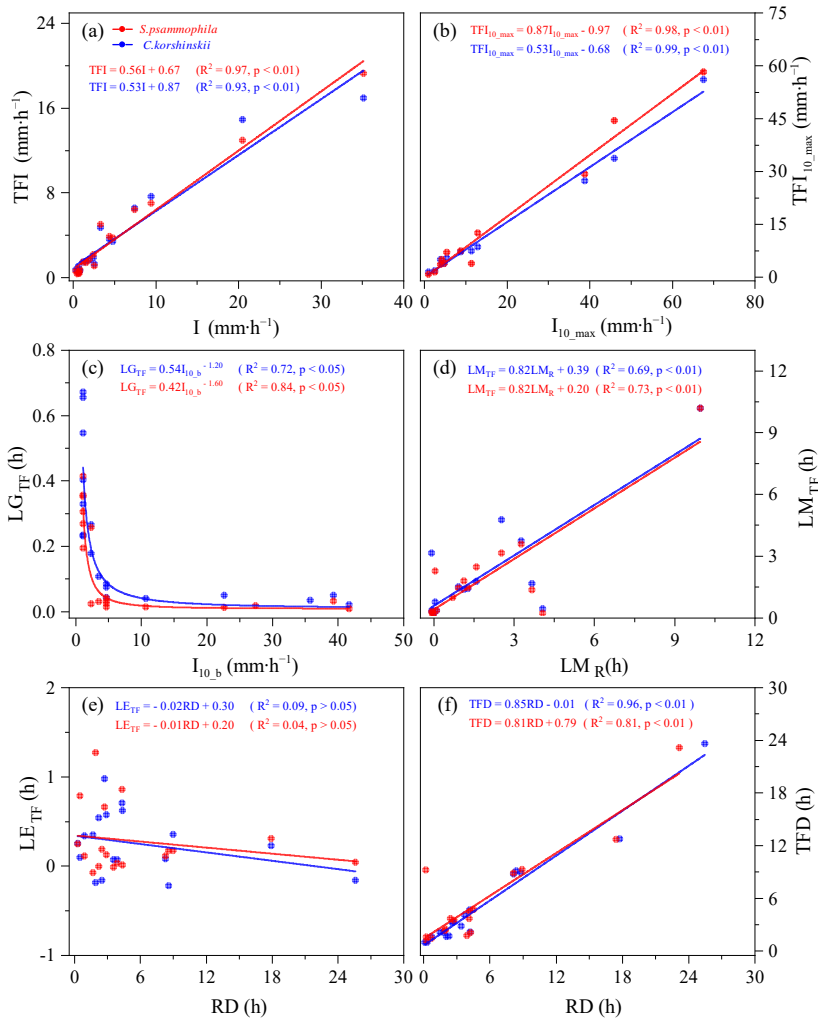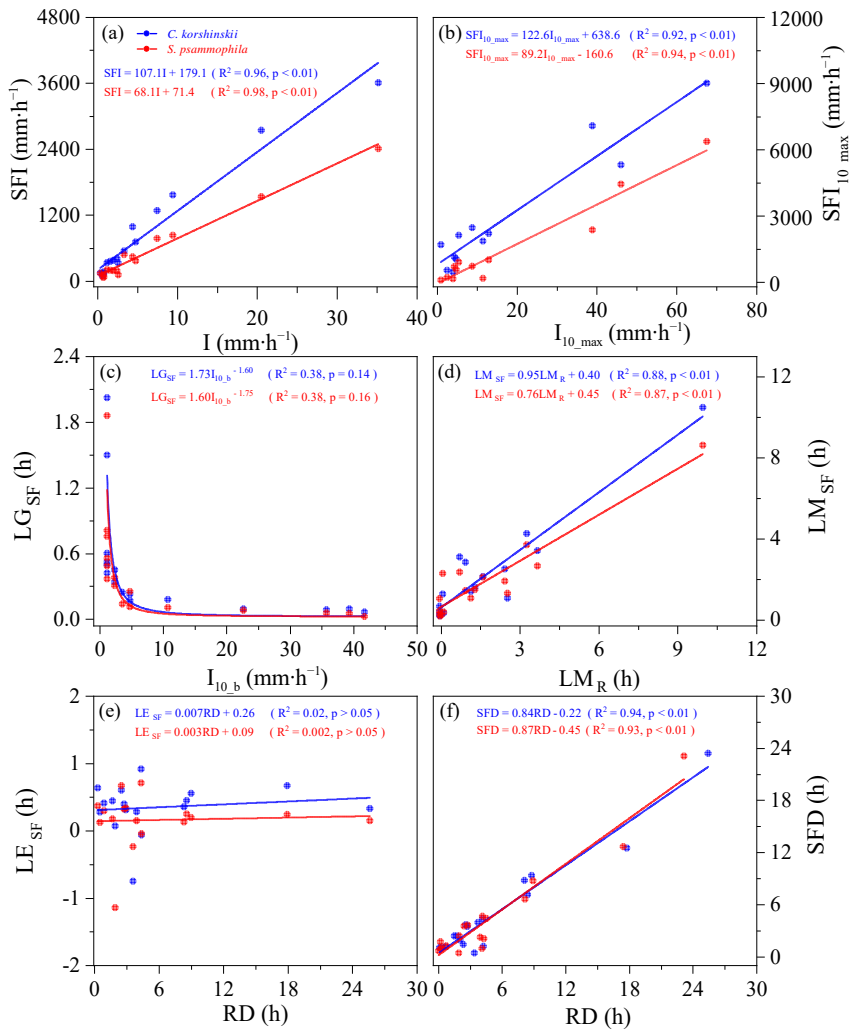
**Figure 6.** Intra-event TF (a, c) and SF (b, d) variables of *C. korshinskii* and *S. psammophila*.

All the variables are explained in Table 2.

**Figure 7.** Relationships of intra-event throughfall variables with meteorological characteristics for *C. korshinskii* and *S. psammophila*. All the variables are explained in Table 2.

830

835

**Figure 8**. Relationships of intra-event stemflow variables with meteorological characteristics

for *C. korshinskii* and *S. psammophila*. All the variables are explained in Table 2.